AD_____

GRANT NUMBER: DAMD17-94-J-4367

TITLE: Development of an Inverse Technique to Estimate the Ultrasound Field During Chest Wall and Breast Hyperthermia

PRINCIPAL INVESTIGATOR: Charles L. Thomas, Ph.D.

CONTRACTING ORGANIZATION: University of Utah
Salt Lakec ity, Utah 84112

REPORT DATE: August 1997

TYPE OF REPORT: Annual

PREPARED FOR: Commander
U.S. Army Medical Research and Materiel Command
Fort Detrick, Frederick, Maryland 21702-5012

REPORT DOCUMENTATION PAGE

1. AGENCY USE	2. REPORT DATE	3. REPORT TYPE AND DATES COVERED
	August 1997	Annual (1 Aug 96 - 31 Jul 97)

4. TITLE AND SUBTITLE

Development of an Inverse Technique to Estimate the Ultrasound Field During Chest Wall and Breast Hyperthermia

5. FUNDING NUMBERS
DAMD17-94-J-4367

6. AUTHOR

Charles L. Thomas

7. PERFORMING ORGANIZATION NAME AND ADDRESS

University of Utah
Salt Lake City, Utah 84112

8. PERFORMING ORGANIZATION REPORT NUMBER

9. SPONSORING/MONITORING AGENCY NAME AND ADDRESS

U.S. Army Medical Research and Materiel Command
Fort Detrick
Frederick, Maryland 21702-5012

10. SPONSORING/MONITORING AGENCY REPORT NUMBER

11. SUPPLEMENTARY NOTES

12a. DISTRIBUTION/AVAILABILITY STATEMENT

Approved for public release; distribution unlimited

12b. DISTRIBUTION CODE

13. ABSTRACT

It is the goal of this research to provide improved numerical modeling of ultrasound propagation through breast tissue and the post mastectomy chest wall for use in patient treatment planning for hyperthermia cancer treatments. Progress in the third year has included the development of a 3D ultrasonic attenuation mapping technique based on signals collected from a modified medical B-scan unit, partial development of a patient registration and tissue geometry acquisition system based on the same B-scan hardware, and investigation of the accuracy of thermocouple measurements to determine ultrasound power incident at a point in tissue. The numerical model developed in the second year was packaged into a convenient usable form during the third year, and alternative inverse optimization techniques were investigated.

14. SUBJECT TERMS			15. NO. OF PAGES
Breast Cancer			28
			16. PRICE CODE
17. SECURITY CLASSIFICATION OF REPORT	18. SECURITY CLASSIFICATION OF THIS PAGE	19. SECURITY CLASSIFICATION OF ABSTRACT	20. LIMITATION OF ABSTRACT
Unclassified	Unclassified	Unclassified	Unlimited

FOREWORD

Opinions, interpretations, conclusions and recommendations are those of the author and are not necessarily endorsed by the US Army.

____ Where copyrighted material is quoted, permission has been obtained to use such material.

____ Where material from documents designated for limited distribution is quoted, permission has been obtained to use the material.

____ Citations of commercial organizations and trade names in this report do not constitute an official Department of Army endorsement or approval of the products or services of these organizations.

____ In conducting research using animals, the investigator(s) adhered to the "Guide for the Care and Use of Laboratory Animals," prepared by the Committee on Care and Use of Laboratory Animals of the Institute of Laboratory Resources, National Research Council (NIH Publication No. 86-23, Revised 1985).

____ For the protection of human subjects, the investigator(s) adhered to policies of applicable Federal Law 45 CFR 46.

____ In conducting research utilizing recombinant DNA technology, the investigator(s) adhered to current guidelines promulgated by the National Institutes of Health.

____ In the conduct of research utilizing recombinant DNA, the investigator(s) adhered to the NIH Guidelines for Research Involving Recombinant DNA Molecules.

____ In the conduct of research involving hazardous organisms, the investigator(s) adhered to the CDC-NIH Guide for Biosafety in Microbiological and Biomedical Laboratories.

3-11-98

PI - Signature Date

Table of Contents

Introduction

This document reports the progress in the third year of a four year grant. This introduction includes a brief description of the subject, goals, and scope of the research project, along with a description of the relationship of this work with that of previous researchers. Following this description is a milestone chart and an outline of the progress to date. (This would be a good place to start for a brief overview of the current program status.) The introductory section ends with a more detailed review of the results of the first two years of the program. The main body of the report is a detailed description of the accomplishments during the third year of the program. This is followed by some concluding remarks summing up the current state of the research and future tasks to be accomplished.

Program Description and Goals

Hyperthermia has been shown to be an efficacious adjuvant therapy in the treatment of recurrent breast cancer.[1,2,3] One of the most flexible and proven methods to induce hyperthermia is ultrasound. In order to optimally utilize such clinical devices it is essential that the operator have the ability to accurately plan a treatment. The clinical hyperthermia situation is diagrammed in Figure 1. A treatment plan consists of a defined motion path and applied transducer power that will raise the temperature of the tumor to a desired set point for a specified time while minimizing the effect on surrounding tissue. The treatment plan must be adjusted for tissue geometry, absorption, and desired temperature history specific to each patient. Planning a treatment begins with the accurate estimation of the absorbed power field created by the ultrasound transducer. Thus, the ability to accurately estimate this field is critical to producing a proper and effective treatment plan.

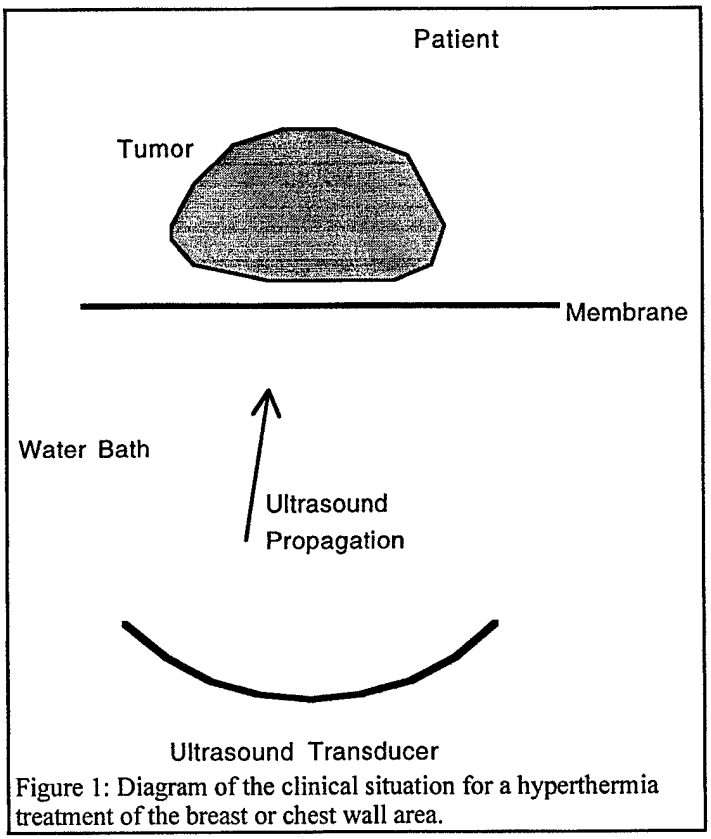

Figure 1: Diagram of the clinical situation for a hyperthermia treatment of the breast or chest wall area.

It is the goal of this research to provide improved numerical modeling of ultrasound propagation through breast tissue and the post-mastectomy chest wall for use in patient treatment planning of hyperthermia cancer treatments. With this improved model the clinician can plan an ultrasound hyperthermia treatment so as to produce the required thermal dose while minimizing patient pain due to excessive temperature or ultrasound-tissue interactions. A clinical system is being constructed to combine model results with experiments in an inverse technique to estimate the absorbed power field in the breast and chest wall during ultrasound hyperthermia. This improved planning will aid the clinicians in providing better hyperthermia treatments, which will improve treatment response rates.

The system under development consists of the following subsystems:

1. An ultrasonic B-mode imager based clinical data acquisition system used to obtain patient anatomy and measure the attenuation of ultrasound by the body tissue.

2. A clinical technique using an ultrasound treatment system to directly measure absorbed power at specific points.
3. An improved model of ultrasound propagation through breast tissue.
4. An inverse technique that integrates experimental measurements and modeling results to obtain the "best" prediction of the ultrasound power deposition field.

The B-mode diagnostic ultrasound imager in Subsystem 1 is used to construct a geometric model based upon each patient's anatomy and to measure the ultrasound attenuation coefficient at selected areas within the tissue region. In Subsystem 2 the clinical treatment system is used in a scanning protocol to locate thermocouples imbedded in the breast tissue. The response of these thermocouples to the scanned ultrasound gives a direct measure of the power deposition at that point. Subsystem 3 is an ultrasound propagation and power deposition model. For this model we have considered 2 options:

a) Hybrid Green's Function Model - Ultrasound propagation from the transducer into the breast is modeled with a hybrid of Green's function solutions used in the homogenous water region and a finite element solution of the acoustic wave equation in the inhomogeneous breast region.

b) Parabolic Model - This is a forward marching parabolic model that is quite fast, but does not take into account reflected energy at interfaces.

Subsystem 4 is an iterative inverse technique that optimizes the parameters of the power deposition model by forcing the model results to match the experimental measurements. The model is used to predict the power deposition at the thermocouple locations, the error between model and experiment is measured, and the error values are used to adjust the model parameters for the next iteration.

This improved power deposition model will be useful in the development of more accurate path planning for hyperthermia treatment. As such it will provide a clinically useful tool that can serve as the base for the development of more accurate treatment path planning, more accurate control techniques, and eventually, higher success rates in hyperthermia treatment with reduced patient discomfort during treatment.

Task Description and Milestones:

	Quarter															
Task Description and Milestones:	1	2	3	4	5	6	7	8	9	10	11	12	13	14	15	16
Finite Element Model	x	x	x	x	x	x	x	x								
Hybrid Green's Function Model					x	x	x	x	x	x						
Parabolic Model					x	x	x	x	x	x	x	x				
Inverse Technique	x	x							x	x	x	x	o	o	o	o
Ultrasonic Hardware Development	x	x	x	x												
Attenuation Measurement 1D			x	x	x	x	x	x								
Attenuation Measurement 3D									x	x	x	x	x	x	o	
Geometry Acquisition/Registration									x	x	x	o	o	o	o	o
in vivo SAR technique	x								x	x	x	x	o	o	o	o
System Integration/Phantom Tests										x	x	x	o	o		
Clinical Data Gathering												x	o	o	o	o

Outline of Accomplishments:

1st Year Accomplishments:

Subsystem 1: Geometry Acquisition and Attenuation Measurement

- Acquisition of ultrasonic B-scan instrument.
- Development of interface hardware to isolate analog A-line information.
- Acquisition of high speed A/D system and development of control software.
- Investigation of reflection based acoustic attenuation measurement techniques.

Subsystem 2: Experimental SAR Measurement

- Initial discussions and verification of equipment.

Subsystem 3: Model Development

- Development and testing of a 2D finite element based model.
- Identification of alternative solutions.

Subsystem 4: Inverse Technique

- Initial discussions.

2nd Year Accomplishments:

Subsystem 1: Geometry Acquisition and Attenuation Measurement

- Development of Log Spectral Difference software for measuring the acoustic attenuation from a single A-line.
- Development and testing of a Force/Balance test apparatus for direct measurement of acoustic attenuation.

Subsystem 2: Experimental SAR Measurement

- No work accomplished.

Subsystem 3: Model Development

- Extension of the 2D FE model to three dimensions. Combination of the FE model with an integral method model to improve the speed of the model.
- Development of a 3D parabolic model as a much faster, possibly less accurate alternative.
- Development of a 3D Green's Function model for use as the "gold standard" with which the other models will be compared.
- Initial model comparisons.

Subsystem 4: Inverse Technique

- No progress.

3rd Year Accomplishments:

Subsystem 1: Geometry Acquisition and Attenuation Measurement

- Laboratory hardware was developed to provide 3D scanning capability for the medical B-scan imager. Clinical hardware is now essentially complete.
- Software to produce a 3D, tissue attenuation map from the A-mode signals was completed and is undergoing verification testing.

- Software and hardware for clinical patient geometry acquisition is approximately 50% complete.

Subsystem 2: Experimental SAR Measurement

- Thermocouple based beam plots have been performed to calibrate the ultrasound power field in water for specific transducers.
- Experiments have been conducted in water and are beginning using cast agar phantoms.
- Preliminary in-vivo experiments were conducted on a dog.
- A finite difference model has been constructed to help interpret the experimental measurements.

Subsystem 3: Model Development

- The parabolic model has been selected for use in regions of low acoustic contrast. In these regions the model is quite fast and loses little accuracy when compared to the Green's Function Model. The Green's Function Model can be used in high contrast areas (close to ribs, etc.)
- An interface has been built for the model which allows the user to specify the volume modeled, the acoustic power input as a 2D complex pressure function, and the model parameters; density, sound velocity, and absorption at each node within the volume.

Subsystem 4: Inverse Technique

- Basic algorithm development is complete. Optimization runs have been completed on simple geometries.

First Year Summary

The first year efforts centered on initial development of the ultrasound propagation models and acquisition and initial development of the diagnostic ultrasound equipment. A brief discussion of these efforts is included below. For more detailed information refer to the first year progress report.

Initial modeling efforts focused on two potential methods: a Green's Function Method where the transducer face is modeled as a distribution of point sources, and the Finite Element Method where FE techniques are used to solve the acoustic wave equation. A two dimensional FE code was written, and verification runs were under way at the end of the first year. The results of these runs and further investigation of the modeling possibilities led to the development of a hybrid model that combines the features of the two techniques to provide improved speed and accuracy. Details of this model are discussed in the second year accomplishments below.

During the first year a diagnostic ultrasound B-mode imager was acquired. This imager was modified to allow access to the raw RF waveform (A-line) for each scan line of the B-mode image. A schematic of the resulting system is shown in Figure 2. The ultrasound unit (Scanner 250, Pie Medical USA 3535 Route 66, Neptune NJ 07753) was modified to output the RF signals along with sync signals. A custom hardware selection device was constructed to read these signals and output a single A-line. A PC based data acquisition system was acquired that allows digitization of the A-line signals. Once the data is in the PC, it is available for use in

software techniques to estimate the ultrasonic attenuation field in the tissue. Along with the hardware development, software was developed to operate the hardware and perform the attenuation estimate.[4]

Second Year Accomplishments

Subsystem 1: Ultrasound Based Anatomy and Attenuation Measurement

Ultrasonic Attenuation Measurement

The power deposited at a specific point in tissue by the ultrasound transducer depends on the intensity of the sound field at that point and the absorption coefficient of the tissue at that point. Clearly, the intensity at a point depends on the initial intensity and the attenuation of the signal in the tissue. This attenuation is due to scattering, absorption, and geometric attenuation. Previous research has shown that the attenuation is highly variable within human body tissue, with measurements varying significantly for different tissue types, for similar tissue on different subjects, and even for the same tissue on the same patient on different days.[6-9] Thus, it is important to measure the attenuation of the ultrasonic signal *in vivo* on the patient at the treatment site.

Using the data acquisition system shown in Fig. 2, it is possible to estimate the attenuation of the ultrasound at different points in the patient tissue from the RF signal collected. This is accomplished using a Log Spectral Difference technique.[7,8,10] Details of this technique are discussed in the second year progress report. It is important to note that Log Spectral Difference is one of several possible techniques and provides an *estimate* of the attenuation.[5] For this

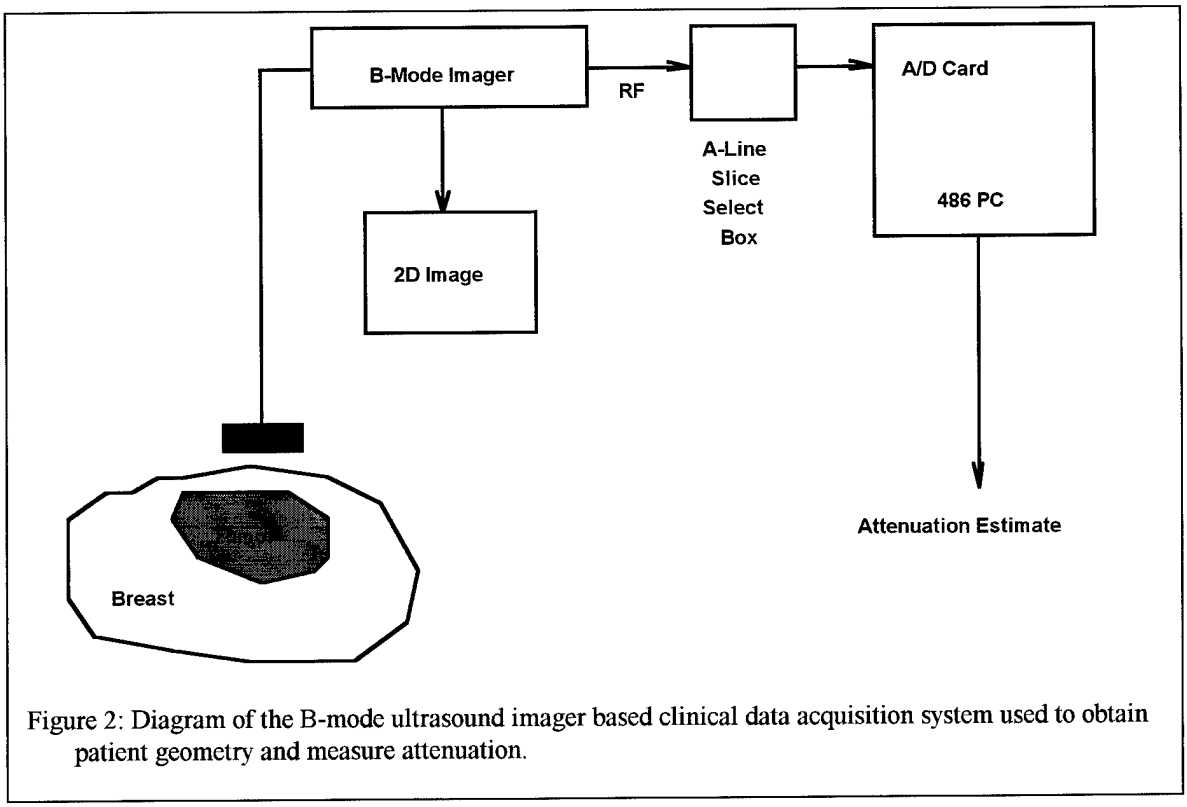

Figure 2: Diagram of the B-mode ultrasound imager based clinical data acquisition system used to obtain patient geometry and measure attenuation.

reason it is important to test the accuracy of the technique with other measurements.

Tests were conducted where the acoustic attenuation of a series of samples were measured using both log spectral difference and the Force Balance technique. Using the Force Balance technique the force generated when an acoustic wave impinges on an absorbing material is measured and related to the power of the wave. Using this technique it is possible to make a direct measurement of the attenuation or absorbed power. For this reason, the force balance technique is used as a standard to which the log spectral difference measurements are compared. While it is generally considered accurate and reliable, the force balance technique is not suitable for use in the clinical experiments due to geometric constraints.

Using the techniques described above, initial tests have been run on chicken breast to compare the results of the two techniques discussed above. Using the Log Spectral Difference Technique, the normalized attenuation coefficient for the chicken was measured as 0.1608 *Nepers x* cm^{-1} *x* MHz^{-1}.[4] Using the Force Balance system measured values ranged from 0.108 to 0.138 *Nepers x* cm^{-1} *x* MHz^{-1}. These values are of the same magnitude as values reported in the literature (0.06 - 0.13 *Nepers x* cm^{-1} *x* MHz^{-1}).[11]

Subsystem 2: Absorbed Power Measurement

No work accomplished in year 2.

Subsystem 3: Ultrasound Propagation Modeling

During the second year two competing models were developed and compared. The first model was a hybrid numerical model using integral methods to solve for the acoustic displacements in the region where the ultrasound propagates from the transducer to the patient's skin and using a finite element solution of the wave equation for propagation in the body. The model predicts the displacements and stresses propagating through the tissue, automatically accounting for reflections and transmission at all interfaces. This model was expected to be quite accurate. A second model, based on the parabolic equation was also developed. This model accounts for forward scattering and refraction, but ignores reflections. It was expected to be much faster, but it was unclear if this model would provide sufficient accuracy.

Results: Hybrid Model

The Hybrid Finite Element model presented two difficulties:

1. To keep the computational time reasonable, it was necessary to model a relatively small volume. It was not possible to produce boundary conditions at the edge of the volume that approximated free space and the model results included significant standing waves generated at the model boundaries. Expanding the model to include the entire chest cavity would solve this problem, but the model would become unmanageably large.
2. Initial tests were performed at reduced frequency with success. When frequencies corresponding to the treatment transducers were used, the finer mesh required resulted in extremely high computation times.

Results: Parabolic Model

The parabolic equation method is an efficient method for modeling acoustic wave propagation through low contrast acoustic materials. This solution technique is somewhat more of an approximation than the hybrid model, but because of the geometry used in the hyperthermia experiment, and the relatively low contrast of breast tissue, it is possible to utilize this efficient approximation. The parabolic model was found to be computationally 8 time more efficient than the Green's function model and 64 times more efficient than the hybrid model.

Figures 3 and 4 demonstrate the kind of information available from the models. In Figure 3 we see a continuous plane wave propagating from the left, entering the body through a vertical skin layer. The wave travels through an elliptical fatty region and into the spherical tumor. The top figure shows the wave energy density that tends to get weaker as the wave moves to the right. Note that the tumor absorbs most of the wave energy resulting in a "dark" shadow behind the tumor. The bottom figure shows the energy absorbed. Note that in the water and normal tissue the absorbed energy is low; even when the wave energy is high. There is an increase in absorbed energy as the wave passes into the tumor. This results from the higher absorption coefficient in the tumor. This effect is shown more clearly in Fig. 4 which is a line plot of the absorbed energy along a central axis in Fig. 3.

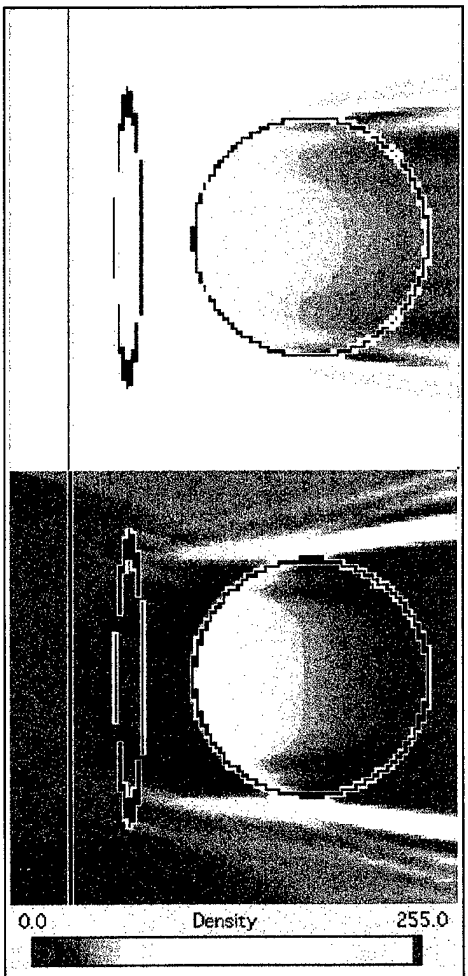

Figure 3: The upper image is the incident energy density. The lower image shows energy absorbed by the tissue.

Model Accuracy

To test the accuracy of the parabolic method, results were compared to an integral equation solution of the same problem that is representative of the best models currently in use. The following figures demonstrate the agreement between the integral equation method and the parabolic method. Figure 5 shows the geometry used for this analysis. Figure 6a shows a color mapped representation of a slice of the field. Figure 6b is an axial plot of the same data. Figure 7a and 7b show the results using a speed of sound in the sphere significantly less than and significantly greater than that of water. Given the differences in the two models, one would

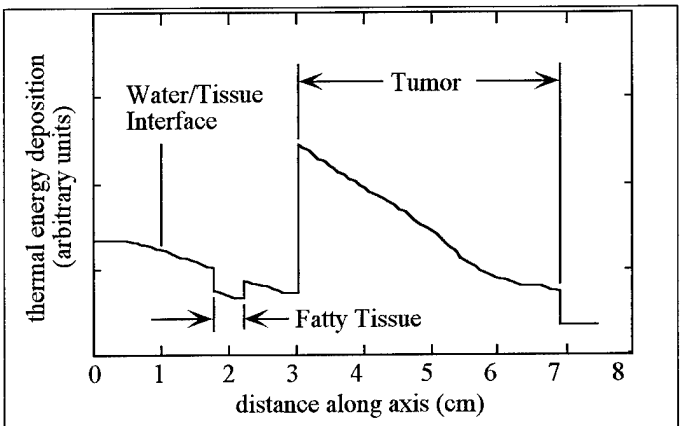

Figure 4: Thermal energy deposition along a central axis predicted by the parabolic model.

expect error to increase as the mismatch in sound velocity between the tumor and water increases. Thus, these two conditions should represent worst case errors.

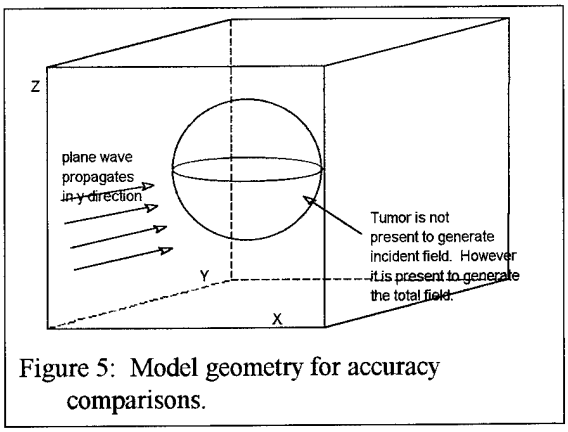

Figure 5: Model geometry for accuracy comparisons.

The excellent match between the two models in the forward scattered diffraction patterns shown in Fig. 7 and the poor match in the reflected diffraction pattern shown in Fig. 6b highlight the differences between the two models. The excellent overall match between the two models in these worst case conditions, coupled with the speed provided by the parabolic model make it an excellent candidate for our application.

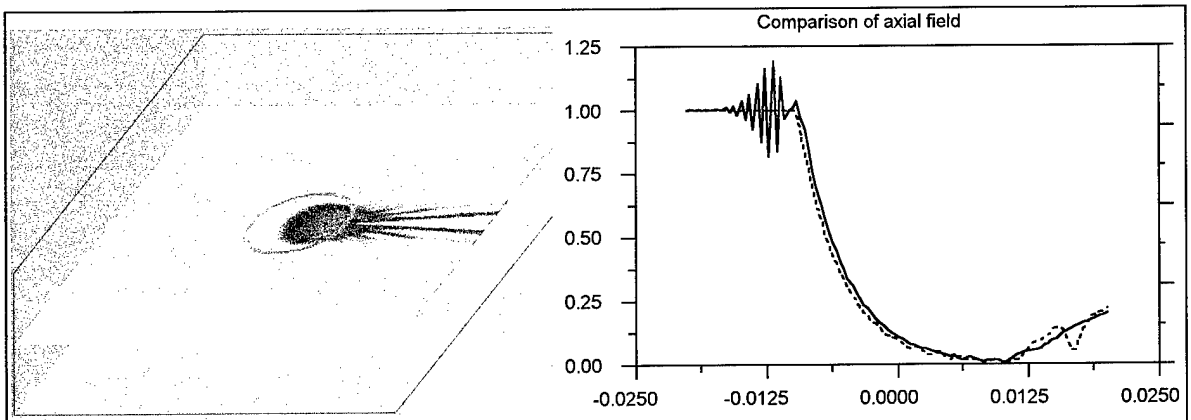

Figure 6: a) Color mapped image of the power deposition in the model from Fig. 5.
b) The integral equation is shown in solid, and shows the diffraction pattern due to reflections from the hard sphere. This plot shows quantitatively that the parabolic method does not take into account the reflections of sound waves. Conditions for this graph correspond to those in Fig. 7b.

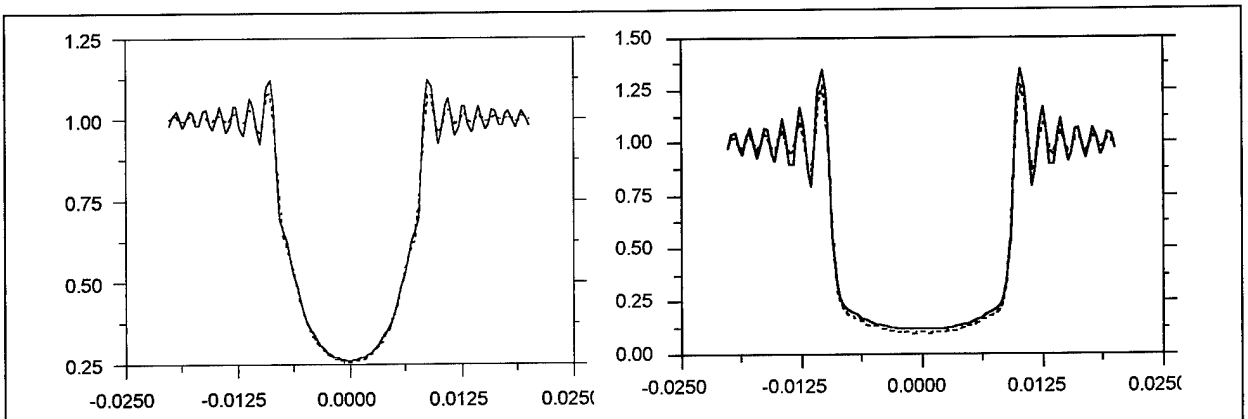

Figure 7: a) The speed of sound internal to the sphere was 1267.7 m/sec, substantially less than that which would be encountered in the breast, thereby making the impedance contrast quite a bit larger than is likely to be encountered in practice. b) Here, the speed of sound internal to the sphere was 1677 m/sec, which is substantially greater than any tumor that would be found in the breast. In each case the solid line represents the integral model and the dashed line represents the parabolic model.

Subsystem 4: Inverse Optimization Technique

No work accomplished during the 2nd year.

Third Year Accomplishments

Subsystem 1: Ultrasound Based Anatomy and Attenuation Measurement

- Laboratory hardware was developed to provide 3D scanning capability for the medical B-scan imager. Clinical hardware is now essentially complete.
- Software to produce a 3D, tissue attenuation map from the A-mode signals was completed and is undergoing verification testing.
- Software and hardware for clinical patient geometry acquisition is approximately 50% complete.

Patient Geometry Acquisition and Registration

The goal here is to be able to place a patient in a known, repeatable location on the treatment station and, using the B-scan imager, identify the geometric structure of the tissue and tumor in the region under treatment. The proposed solution to this problem has evolved significantly since the initial proposal. In the initial proposal CT data and printed B-scan images were to be converted into a geometric description of the treatment region suitable for use by the math model. This has evolved into specific hardware and software that make up a clinical system that is described below. The hardware for this system was not included in the original proposal and we are currently using borrowed equipment and awaiting approval to purchase equipment that will be dedicated to this work. During this reporting period, the software for the system described below was developed and is currently approximately 50% finished.

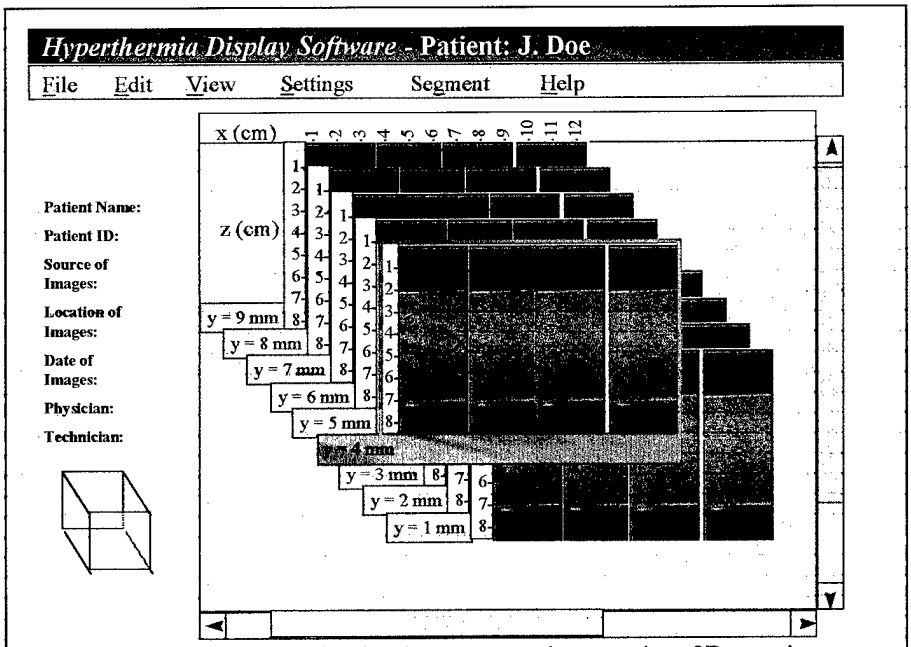

Figure 8: The software under development acquires a series of B-scan images, tiles them together creating a larger 2D image, and coordinates the display of the 2D images to represent 3D geometry.

Clinical System Description

The patient positioning system consists of several integrated steps. The first step is to reproduce the laser positioning system used for radiation therapy. Use if this positioning system will

allow CT scans taken by the radiologist to be used for added reference. The system requires three collimated, wall-mounted lasers that are aligned with points marked by freckle-sized tattoos on the patient's skin. After the patient is initially positioned, the laser spots on the patient's skin are marked with tattoos. The patient position is checked in later treatments by observing the position of the laser spots with respect to the tattoos. The hyperthermia treatment apparatus at the University of Utah currently is equipped with two wall-mounted lasers and a third is planned.

In the second phase of positioning the patient, a series of B-scan ultrasound images of the treatment area are collected. These images are used to identify the locations of thermocouples, interfaces between different tissue types, and other anatomical features within the region that will be affected by the hyperthermia treatment. The B-scan images are digitized using a video capture card. A custom software, developed as part of this research, coordinates multiple B-scan images into a series of slices representing the 3D patient geometry. A screen capture from this system is shown in Figure 8.

The doctor or technician traces features of the B-scan images that are of interest. Using an attenuation map developed using a process described below as a reference, the different regions identified by the tracings are assigned attenuation values. The software processes this information and produces a 3D grid of nodes where each node is assigned appropriate values to represent the patient geometry for processing by the math model. Figure 9 demonstrates this process.

The left most image contains 3 B-scans that have been registered and combined, producing a single image. In the center image, the doctor or technician has mouse sketched different regions. In the right most image, these regions have been assigned different acoustic properties based on apriori knowledge and information from the attenuation mapping system discussed below.

The following outline describes the anticipated clinical procedure using the developed system. Depending on the time required to complete the inverse optimization procedure, the patient may either lay in position and wait, or be released and return for treatment hours or days later.

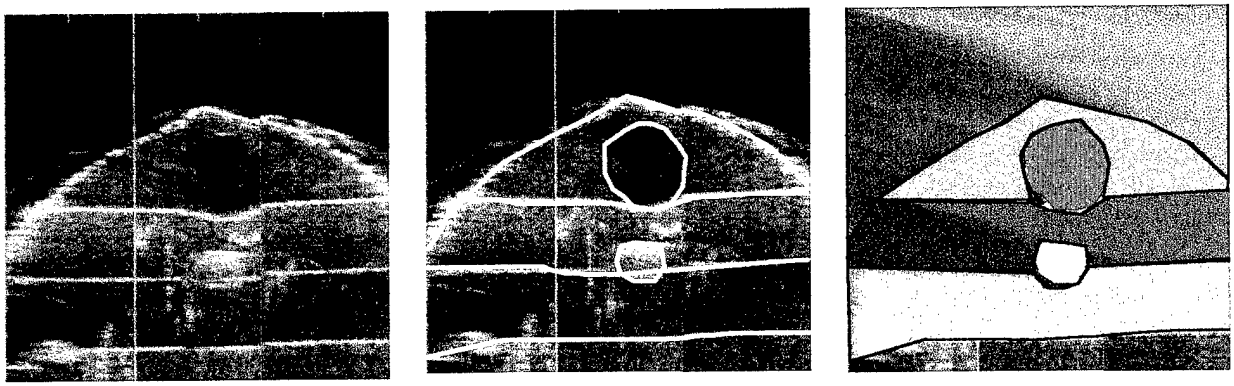

Figure 9: Each image is processed by a doctor or technician. The process involves mouse sketching the borders of identifiable regions and assigning each region uniform acoustic values estimated from an attenuation map.

Patient geometry acquisition and initial registration:

1. A coordinate system with a zero point near the tumor is usually defined by the radiologist. This zero point can be located by aligning wall-mounted lasers with three small tattooed marks on the patients skin or with marks on a mold used to hold the patient in position during the treatment. Align the patient at the zero point.
2. Center the B-scan around this zero point and scan the transducer in order to capture a "grid" of two-dimensional images that have known locations with respect to the zero point.
3. Use a frame grabber to store the images. The location of the scan with respect to the zero point must be recorded with each image.
4. Trace interfaces and loops that represent different tissue regions. Mark thermocouple positions.
5. Store these traces in an image that has the same scale and position as the original image.
6. Use attenuation information to define the tissue properties within the traced regions.
7. Format data and output to optimization software.

Repositioning patient for treatments:

1. Align wall-mounted lasers with marks on the patient's skin.
2. Scan the anatomical region to be treated with an ultrasound B-scan transducer using the same grid pattern used in the initial geometry acquisition scan.
3. Use a frame grabber to store the images and their location with respect to the zero point.

4. Compare the captured images to those from previous scans to verify that thermocouples and markers on the skin are in the same locations in the corresponding images. Adjust patient position until the images show that the thermocouples and markers are in the correct locations.

Three-dimensional Ultrasonic Attenuation Field Measurement

As mentioned above, the goal of this research is to produce a model that will accurately predict the power deposited at all points in a region of tissue, during a hyperthermia treatment. This will allow the physician to develop a better treatment plan that will maximize the positive effects and minimize pain and other adverse effects. In order for the inverse model to accomplish this efficiently, the model must begin with model parameters that are "in the ball park" of the final optimal values. The least well known of these parameters is the acoustic attenuation of the tissue. Thus, a technique is developed here that will predict the acoustic attenuation field within the tissue based on data from a B-scan imager. The third year efforts have extended the previous accomplishments to include the ability to produce a 3D attenuation map from a series of B-scan images.

Background

Measurement of ultrasonic attenuation from reflected signals has shown promise of being a valuable diagnostic tool[12-20]. It allows physicians to diagnose illnesses that cannot be diagnosed on a B-mode ultrasound image. Because of this, several methods of calculating the ultrasonic attenuation from reflected signals have been developed [14,17,19-22]. These methods were then used to calculate the global attenuation of a structure. The next step in attenuation calculation was to produce an attenuation image that could be used in conjunction with the B-mode image. Walach and others have developed techniques that relate a two-dimensional B-mode image to a two-dimensional attenuation image or map [12,13,23]. Seeing both images side-by-side, the physician has an increased diagnostic capability.

However, the usefulness of an attenuation map is not limited to diagnostics. A 3D attenuation mapping technique has been developed here that not only provides the initial estimates for the power deposition model. But has potential to produce enhanced resolution 2D attenuation images.

Method

In order to build the three-dimensional attenuation map, a B-mode imaging transducer was placed on a two-dimensional linear motion machine. The transducer is part of an ultrasonic imaging system (PIE Scanner 250) which provides access to the reflected ultrasound signal (A-line), before processing, as well as synchronization signals to give the location of the waveform along the width of the transducer. With this in place, software was developed that scanned the transducer to cover the entire geometry of the structure being modeled, while collecting and organizing the data. This is the same data shown in Figures 8 and 9 collected by the patient registration system, except that the raw A-lines are recorded.

The data was collected with an eight-bit analog to digital converter, and was then written to disk. A technique has been developed that uses several different gain settings for each collection to mimic a higher-precision conversion. Using this technique, each A-line was analyzed at the highest possible gain setting where saturation did not occur. The focus of the transducer was set so that the structure being analyzed was in the far field of the transducer. This insures that diffraction effects in the near field do not enter into the calculations. Once the data was collected it was then analyzed to produce the attenuation map.

The log spectral difference method was used to estimate the slope of the attenuation to frequency relationship. (Lyons and Parker found that for most soft tissues, the attenuation was related to frequency to the power of n, where n is equal to 1.0 - 1.3 [25]. The value for n was set to 1 in this research.) This method utilizes the ratio of the power spectrum from a shallow and deep segment of the region of interest (see Figure 10) to compute the attenuation slope for that region. The specific steps of this technique have been presented in the 2nd year progress report as well as previously in the literature and will not be discussed here [14,15,22,26]. Our application of this method for the production of a 3D, attenuation map will be discussed next.

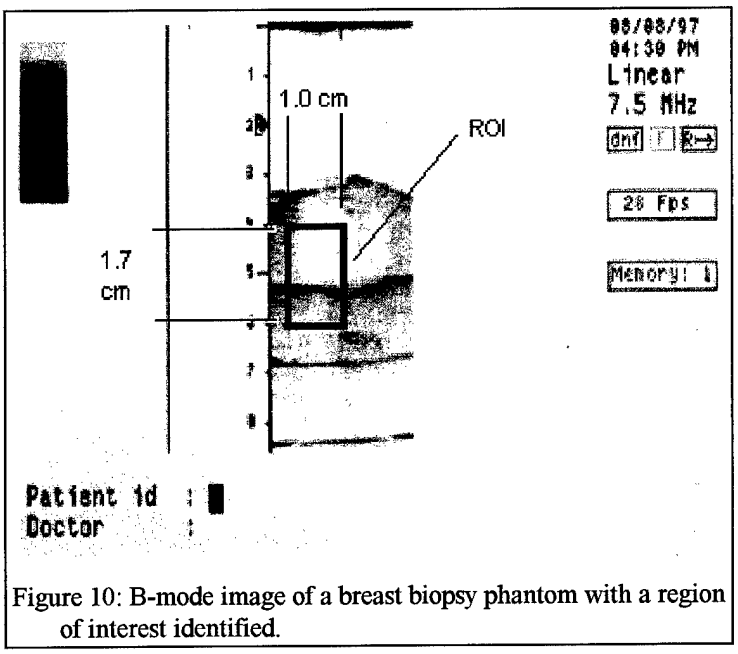

Figure 10: B-mode image of a breast biopsy phantom with a region of interest identified.

As mentioned previously, the log spectral difference technique is a way of estimating the slope of the attenuation for a specified Region Of Interest (ROI). To produce the attenuation map, a ROI of a determined size was moved throughout the three-dimensional data space until an attenuation map was produced. The region of interest selected was 1.0 cm wide and 1.7 cm in depth (see Figure 10). The width was chosen because it allowed the computation to be averaged over ten reflected signals. The depth for the region of interest came from a formula presented by Kuc [26] and the specifications of the transducer. Once the ROI size was selected, it was moved throughout the data space incrementally in 1.0 mm steps in all three directions. The attenuation-slope value for each calculation was assigned to a point in the center of the ROI, thus producing an attenuation map. This 2D ROI is similar to that used by previous researchers. The additional information available from the 3D data collection used here allows a 3D ROI to be investigated, where data from a 3D region are averaged together to improve the accuracy and/or

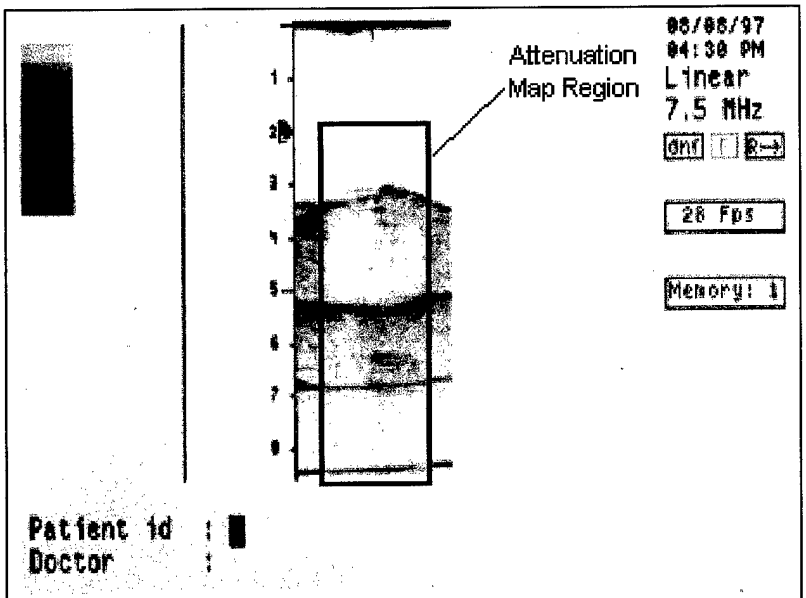

Figure 11: B-mode image of breast biopsy phantom with corresponding region of attenuation mapping outlined.

resolution of the measurement. Software has been developed to completely automate the task of data acquisition and analysis, and calibration tests are underway.

Results

Various tests have been performed to determine the settings that produced the most precise and least noisy attenuation map. Initial tests varied the ultrasound power, gain setting, and whether or not the region of interest should be two-dimensional (space averaged) or three-dimensional (volume averaged). For these preliminary experiments, visual comparison of the attenuation images versus the anticipated attenuation image (obtained from examining the B-mode image) was used to determine the optimal settings.

Preliminary results showed no benefit from the 3D volume averaging. We anticipate that this is due to registration problems in the data collection and we are continuing to investigate. During the analysis of the attenuation images, it was noted that data was lost in areas where the ultrasound back scatter was too low, or too high. For any single gain setting, the data loss was significant. However, based on a visual comparison, other gain settings appeared to produce attenuation images of the almost the same quality, but with data losses in different regions. These observations resulted in the multiple gain setting technique discussed above. This technique has resulted in images with significantly less data loss.

Figure 11 presents a B-mode image of a breast biopsy phantom. This image was taken at the same time that attenuation data was being acquired for the same image space. Because the attenuation slope value is assigned to a point in the center of the ROI, and the because of the size of the ROI, 0.5 cm of attenuation data was lost on each side of the B-mode image. For the same reason, 0.85 cm was lost from the top and bottom of the image. Figure 12 shows the corresponding attenuation map for the region indicated in Figure 11.

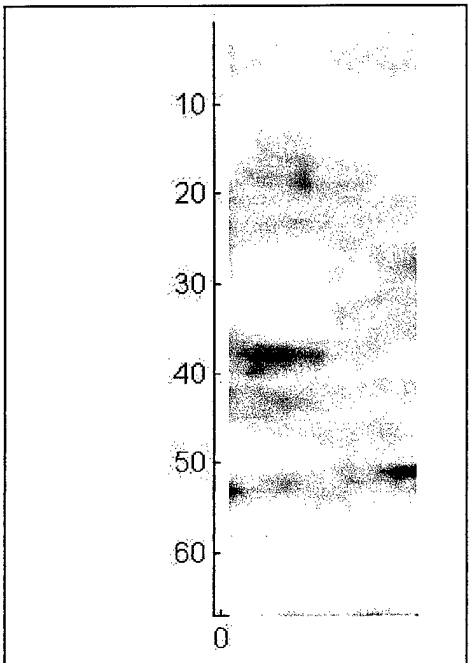

Figure 12: Attenuation image. This image corresponds to the highlighted region in Figure 2. Values of attenuation are in 1/(cm dB MHz).

Discussion

Attenuation maps are not a new application. Walach and others have produced attenuation maps in the past [12,13,23]. However, this application is the first three-dimensional mapping system we have been able to find. This application has limitations similar to the other maps that have been produced. One such limitation is the resolution of the attenuation map.

Most attenuation-calculation techniques require a large ROI in the depth direction. The literature has recommended that the log spectral difference method be used for global attenuation estimation (greater than 5.0 cm) [14,22]. However, Kuc has theorized that this method can be used for smaller regions, but that the size of the ROI has a lower limit. As the length of the ROI decreases below this limit, the noise associated with the application increases dramatically [26]. As can be seen from Figure 12, the

resolution is poor compared to the B-scan image. In addition, the attenuation image only partially matches the expected image (from examining the B-mode image in Figure 11). Experiments using the radiation force balance apparatus developed in the first and second years of the project, are currently under way to quantify the error between the attenuation predicted by this technique and the true attenuation of a sample.

Inhomogeneous regions are another problem with this technique. Several interfaces and varying structures were present in the phantom that was used for calculation. The development of this and other estimation techniques were based on the tissue being homogeneous within the ROI [14,17,18,21,22]. This problem was initially ignored in this study in order to discover how the method would handle interfaces and different tissues within the ROI.. The bright circle in Fig. 11 is a water filled sphere, 1.2 cm diameter. Note that while this sphere is smaller than the ROI it does show up. This is taken as a sign that this method may be used to calculate the attenuation in small tissue structures.

Future Efforts

Clearly interfaces present the opportunity for a variation of attenuation in the two regions separated by the interface. When the ROI overlaps the interface, the attenuation measurement can be expected to be inaccurate. (While it may accurately represent the average of the attenuation within the ROI, we anticipate using the attenuation map to allow a technician to select a representative value for an identified region. In this case we prefer attenuation values that are representative of a single region.) We are currently developing an algorithm to separate "good" data from noisy measurements and anticipate that this will produce larger regions of "lost" data with smaller regions, centered within homogeneous regions, where the results are relatively uniform. This technique is based on an examination of a histogram of attenuation values within a defined neighborhood of each other. Using this technique, attenuation values are only considered valid if the histogram has a single mode, with a standard deviation less than a threshold value. At interface regions bi-modal histograms or large standard deviations are expected.

Another source of error in the three-dimensional map is the location error of the transducer. In tests, the largest error in positioning the transducer found was 0.04 mm. The beam width of this transducer at the focal point is 1.4 mm. Therefore, the positioning error is not considered a significant source of error.

Regardless of the errors involved, the attenuation estimation method should be successful if it can appropriately predict the relationship between the attenuation and the various structures within the phantom or anatomy. (i.e. which regions have "higher" attenuation and which regions have lower attenuation.) This kind of an approach can be taken because of the iterative nature of the inverse model that will use these values.

Subsystem 2: Experimental SAR Measurement

- Thermocouple based beam plots have been performed to calibrate the ultrasound power field in water for specific transducers.
- Experiments have been conducted in water and will begin shortly using cast agar phantoms.
- Preliminary in-vivo experiments were conducted on a dog.

- A finite difference model has been constructed to help interpret the experimental measurements

To accomplish the inverse optimization of the theoretical model, the results of the model must be compared against actual values that are determined by experimental means. The ultrasound propagation model predicts the incident power at all points in the modeled region, as well as the absorbed power. At a given point, these two quantities are related through the local attenuation. Thus, the model can be optimized by comparing the propagation model results to either the incident power or the absorbed power at several points in the model. The experimental values needed for optimization can be determined using the same thermocouples which are inserted for observation of steady state temperature during clinical hyperthermia treatment.

Experimental measurement of the power deposited in tissue at a specific point is not entirely straight forward. Researchers note that the interaction of the thermocouple probe with the ultrasound results in temperature artifact.[24] This artifact results from two sources: viscous heating at the interface between the probe surface and the tissue, and absorption of acoustic energy by the probe its self. The viscous heating is a surface phenomena and results in a small artifact with a short time constant causing a rapid initial temperature rise when acoustic power is initiated. This artifact is usually only noticed when conducting tests using bare thermocouples. Probe sheaths of steel, fused silica, and various plastics have been shown to absorb ultrasound power at a higher rate than tissue. Plastics, the most common sheath materials used in hyperthermia treatment, absorb ultrasound energy at a significantly higher rate than tissue resulting in a significant artifact that is exhibited over a longer time scale than the viscous artifact. The temperature rise in the tissue, a much larger volume than the sheath, occurs over an even longer time scale.

The combined result of these effects is shown in Figure 13. In Figure 13(a), a bare thermocouple was submersed in a water bath and insonified for 0.6 seconds. Note the rapid initial jump followed by a relatively linear region. The initial jump is caused by viscous heating at the thermocouple/water interface and the linear region is established when local conduction between the thermocouple and surrounding water becomes significant. At longer times the temperature rise will become non-linear as larger scale conduction and convection become significant. In Figure 13(b) the experiment

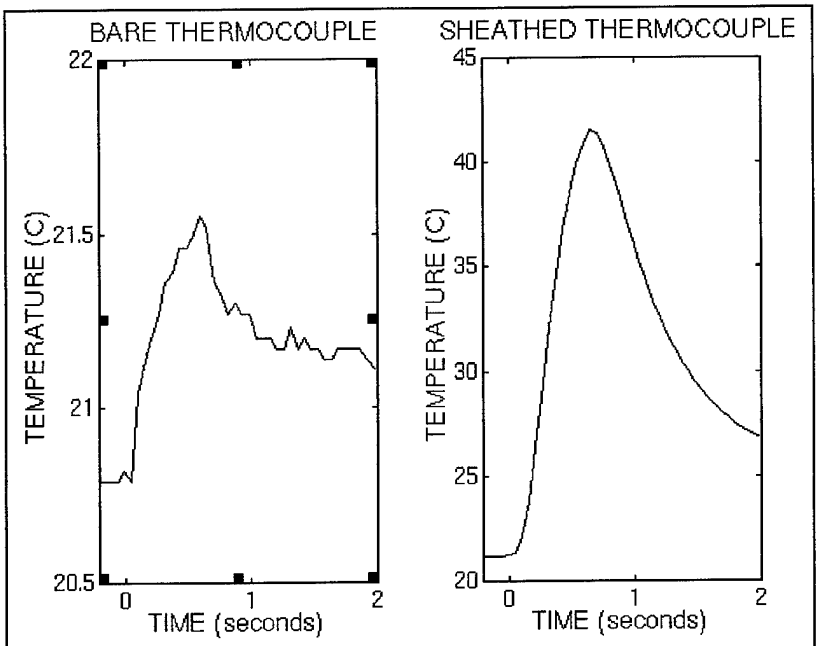

Figure 13: a) Results from a bare thermocouple in water insonified for 0.6 seconds. b) Results from a plastic sheathed thermocouple in water insonified for 0.6 seconds.

was repeated with a sheathed thermocouple. Note that the temperature rise is much more significant, rising roughly 20 degrees in 0.6 seconds compared to less than one degree for the bare thermocouple. This large jump is attributed to the power absorption of the sheath. Any viscous heating that occurs is clearly lost in this rapid temperature rise. The slope of this rise is indicative of the power absorption in the sheath.

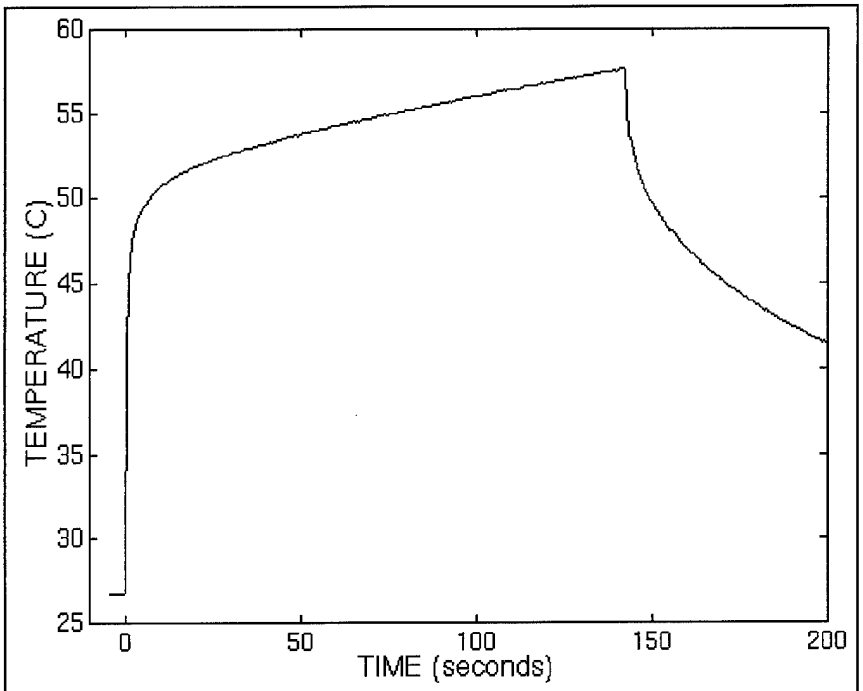

Figure 14: Results from a plastic sheathed thermocouple immersed in water and insonified for approximately 140 seconds.

If the power is applied for a longer time, the rapid initial rise of the sheathed thermocouple is balanced by conduction between the sheath and the surrounding water. This effect is shown in Figure 14. The second linear regime achieved represents the temperature rise of the media surrounding the thermocouple.

In these experiments the thermocouples were immersed in water, a very poor absorber of ultrasound energy. Thus, essentially all of the temperature rise of the water was due to conduction from the thermocouple sheath. In tissue we expect larger absorption directly by the tissue. An actual experiment conducted in tissue will produce results similar to those shown in Figure 15. Here a sheathed thermocouple was inserted in the muscle tissue of the thigh of a dog. The focus of the ultrasound transducer was centered on the thermocouple and the area was insonified for 0.6 seconds at several different power levels. Note that in each case the power was much lower than that used in the experiment from Figure 14, evidenced by the relatively low temperature rise. In future experiments we intend to calibrate the plastic sheath and use it as an incident power sensor, allowing the ultrasound power incident at the thermocouple to be measured.

Modeling the Thermocouple Behavior

In the absence of conduction, power is related to heat generation by the following equation:

$$\rho c_p \frac{dT}{dt} = \alpha I \qquad \text{Equation 1}$$

where ρ is the density, c_p is the specific heat, α is the absorption coefficient, and I is the local intensity of the ultrasound field.

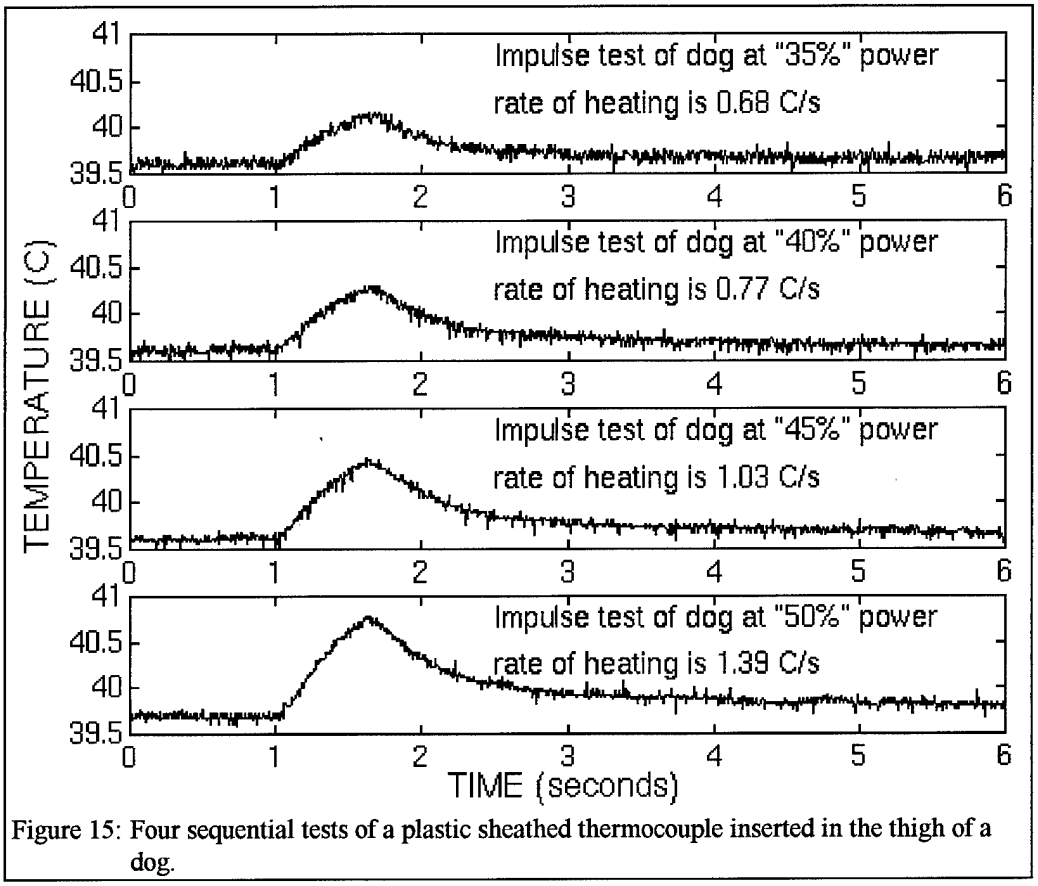

Figure 15: Four sequential tests of a plastic sheathed thermocouple inserted in the thigh of a dog.

If a plastic thermocouple probe and surrounding tissue at uniform temperature is suddenly insonated by ultrasound of constant intensity, the probe and tissue will begin to rise in temperature. The plastic probe will heat more rapidly than the tissue because it has a larger absorption coefficient than the tissue. For a short period of time immediately following insonation, conduction of heat will be small and the rate of temperature rise is dependent solely on the absorption coefficient of the medium being insonated. If the time constant of the thermocouple is sufficiently small the thermocouple, being surrounded by plastic, will reflect the temperature of the plastic. If the absorption characteristics of the thermocouple probe can be sufficiently characterized, the intensity of incident ultrasound can be determined by the temperature vs. time response of the thermocouple to a suddenly applied ultrasound field.

The radial distribution of a focussed ultrasound beam can be closely estimated as a Gaussian function. The following equation describes the radial intensity distribution:

$$I(r) = I_{max} e^{-r^2/\beta} \qquad \text{Equation 2}$$

where I_{max} is the intensity at $r = 0$ and β is a measure of the beam width as determined by a least squares error curve fit. [24]

If the ultrasound is applied for a short duration to prevent significant conduction effects then the temperature distribution produced by the absorption of the ultrasound will also be

Gaussian. Using the theory put forth by Parker, the time dependent temperature at the center of the focal region can be described by the following equation:

$$T(t) = T_{max}/(4kt/\beta + 1) \qquad \text{Equation 3}$$

where k is the heat conduction coefficient of the tissue and T_{max} is the maximum temperature attained at the center of the focal region at the end of ultrasound application.

At the termination of the momentary application of ultrasound the plastic sheathing of the thermocouple probe will be at a higher temperature than the surrounding tissue. However, because the heat capacity of the thermocouple is small compared to the heat capacity of the tissue, excess heat stored in the probe will diffuse into the tissue and the probe temperature will reach equilibrium with the surrounding tissue and follow the temperature decay of the surrounding tissue. Curve fitting the decay of the tissue temperature by the least squares error method the decay can be backtracked and the value of T_{max} determined. T_{max} and the duration of insonation are used with equation (1) and the intensity determined by the rate of heating to determine the absorption coefficient of the tissue.[24]

It has been determined by previous investigators that absorption accounts for 90-100% of attenuation in soft tissue.[25] Therefore it is not completely accurate to compare attenuation determined by B-mode imager and absorption determined by thermocouple probe but an error less than 10% is not unreasonable when compared to other errors likely to exist.

A program was created on the hospital treatment system that positions the transducer, delivers power for a period of time, and records the temporal temperature data from the thermocouple probes. This program is able to attain temperature data from several seven junction probes every 3/100 sec. To test the program a 10 cm, 2MHz transducer was mounted to the positioning gantry and an array of thermocouples was placed in a water bath above the treatment system. The thermocouples were located with the existing thermocouple locate routine. It was found that the positioning system was only able to locate the thermocouples with $\pm$ 2-4cm accuracy. A radial beam intensity plot was attempted beginning 1 cm away from the center of focus and traversing through the focus at 2mm increments. Because of the tight beam focus and lack of positioning accuracy it was found that there was very little correlation between expected position and beam intensity.

To characterize the beam shapes of the available transducers an array of epoxy covered thermocouples was created and oriented perpendicular to the beam axis. The array was moved through the beam transverse to the beam axis in 1mm increments and the steady state temperature was recorded for the thermocouples at several different distances from the face of the transducer. This procedure was followed for the focussed 10cm diameter 2MHz, focussed 7cm diameter 500kHz, unfocussed square 4cm 1MHz, and unfocused 3cm diameter 4MHz transducers. The unfocussed transducers were not characterizable because of the irregular intensity consistent with the long near field of the beams. The 10cm and 7cm diameter transducers had a Gaussian profile in the radial direction at the focus. Least squares error curve fit produced a Gaussian parameter of 0.029 cm^{-2} for the 10 cm diameter transducer and a Gaussian parameter of .42 cm^{-2} for the 7cm diameter transducer.

The 0.029 cm^{-2} Gaussian parameter at the focus of the 10cm diameter transducer creates a beam width of around 6mm. which is too narrow for the accuracy of the hospital positioning system and the steep temperature gradients created by the narrow focus decrease the temporal window during which conduction is insignificant. The 0.42 cm^{-2} Gaussian parameter at the focus of the 7 cm. diameter transducer creates a beam width larger than 2 cm. This larger beam width will create a less steep temperature gradient and lengthen the temporal window for the rate of heating measurement. The longer length of focus of the 7 cm. transducer is also beneficial in avoiding error in the Z-direction.

Finite difference code was written to model a thermocouple probe embedded in tissue. The finite difference model will be used to verify the assumptions and clarify the unknowns of the experimental technique. Verification of the 1-D model is in process after which a 2-D and/or 3-D model will be created.

A considerable amount of phantom testing with the 7cm. diameter transducer will begin shortly. The phantom tests will be designed to prove the accuracy of the rate of heating and thermal pulse decay technique in combination with the probe geometry used in clinical hyperthermia treatment. After verification the procedure will be integrated with the other subsystems of the inverse estimation technique to provide geometric data for the thermocouple probes and local measured power and absorption values.

Subsystem 3: Model Development

- The parabolic model has been selected for use in regions of low acoustic contrast. In these regions the model is quite fast and loses little accuracy when compared to the Green's Function Model. The Green's Function Model can be used in high contrast areas (close to ribs, etc.)
- An interface has been built for the model which allows the user to specify the volume modeled, the acoustic power input as a 2D complex pressure function, and the model parameters; density, sound velocity, and absorption at each node within the volume.

Based on the results of the 2nd year, the parabolic model has been selected for use in regions of low acoustic contrast. In these regions the model is quite fast and loses little accuracy when compared to the Green's Function Model. If necessary, the Green's Function Model can be used in high contrast areas (close to ribs, etc.) The Green's Function Model could be used everywhere resulting in a significantly slower, slightly more accurate result.

During the third, year work on the model has focused on the development of a practical and convenient user interface that will allow the model to be adapted to different transducers and tissue geometries. Toward this purpose, an interface has been built for the model which allows the user to specify the volume modeled, the acoustic power input as a 2D complex pressure function, and the model parameters, density, sound velocity, and absorption at each node within the volume. The model interface, as described below is complete.

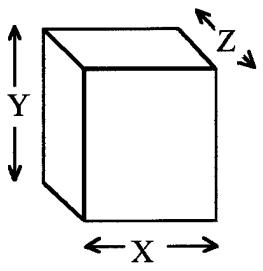

The interface allows the user to specify the dimensions, X, Y, Z of a rectangular volume that will be modeled. The size of the volume to be modeled is limited by the requirement for 2 nodes per wavelength at the transducer frequency under investigation and by the maximum number of nodes that the model can handle. At the current time, the model can handle 1,000,000 nodes. Thus, a volume of 100 by 100 by 100 nodes could be modeled. At 1.5 MHz, this would be a 5 cm cube. It should be noted that larger volumes can be modeled by slicing the volume into 1,000,000 node rectangles and modeling each sequentially.

Within the modeled volume the tissue is characterized by specifying the density, sound velocity, and acoustic absorption at each node. As a result the interface is very general. There is much more flexibility in this interface than is currently required by the inverse optimization scheme. If we later desire to optimize the sound velocity field within the tissue, or the density field, no modifications to the model will be required.

Transducer Model

If the transducer were modeled as part of the above described volume, it would be difficult to fit the desired tissue volume into the limited model volume. This problem is addressed by solving for the complex pressure field created by the transducer being modeled and applying this field at one surface of the model volume.

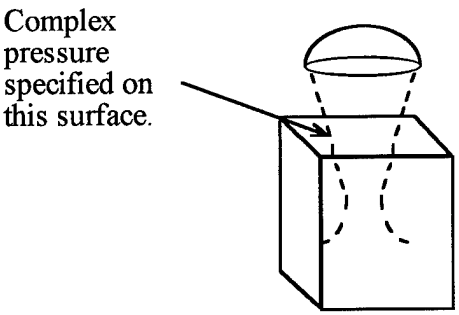

The 3D complex pressure field is first found for the transducer in water. This is done by matching a numerical solution to the results of calibration experiments where the temperature rise of epoxy coated thermocouples is measured in a water bath. Using this data, as long as the edge of the modeled volume extends beyond the skin into the water bath, the effects of the transducer can be modeled accurately by finding the intersection between the planar surface of the model and the 3D pressure field. Note that a single calibration allows the transducer to be positioned anywhere with respect to the model volume.

With this user interface in place, the model can be treated as a black box, where the optimization scheme is ignorant of the details of the model within the box, but simply specifies inputs and collects the output from the model. Once the transducer has been calibrated (or several transducers), the user simply specifies the transducer location and orientation, and the nodal acoustic properties that were identified in Subsystem 1. The model then outputs the acoustic power deposited at each node within the model volume.

Subsystem 4: Inverse Technique

- Basic algorithm development is complete. Optimization runs have been completed on simple geometries.

Inverse Method for Optimizing Tissue Attenuation Values

In the original proposal, it was suggested that three parameters could be allowed to vary between tissue types. The numerical model developed has the capability to change all three parameters. However, in initial trials, it is assumed that speed of sound, (c) and impedance, (Z) are known constants for the tissues with which we will be dealing. Consequently, attenuation is the only parameter that changes between tissue types and, thus, will be the only parameter optimized.

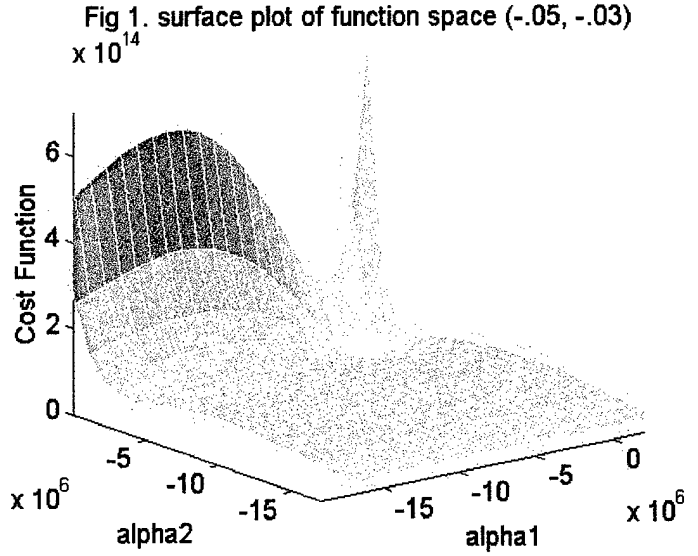

Figure 16: This is a surface plot of an example error function space. The optimization scheme is searching for the minimum in this function.

The method discussed in the proposal uses the Jacobean matrix to adjust the initial parameter values at model nodes and iterates until the error function is minimized. (Here error is some weighted sum of the differences between model predictions and experimental measurements.) This method has been used in initial trials but is being compared to other methods to determine the best method for our model. A second method, the Conjugate Gradient method, is also being evaluated currently.

Initial trials have begun using each of these methods to search for minimum error points in the error function for simple function spaces. Figure 16 shows an example where only two parameters are varied. Given an initial value for the two parameters, each method iteratively searches for the optimum (minimum) point in the function. Essentially the only difference

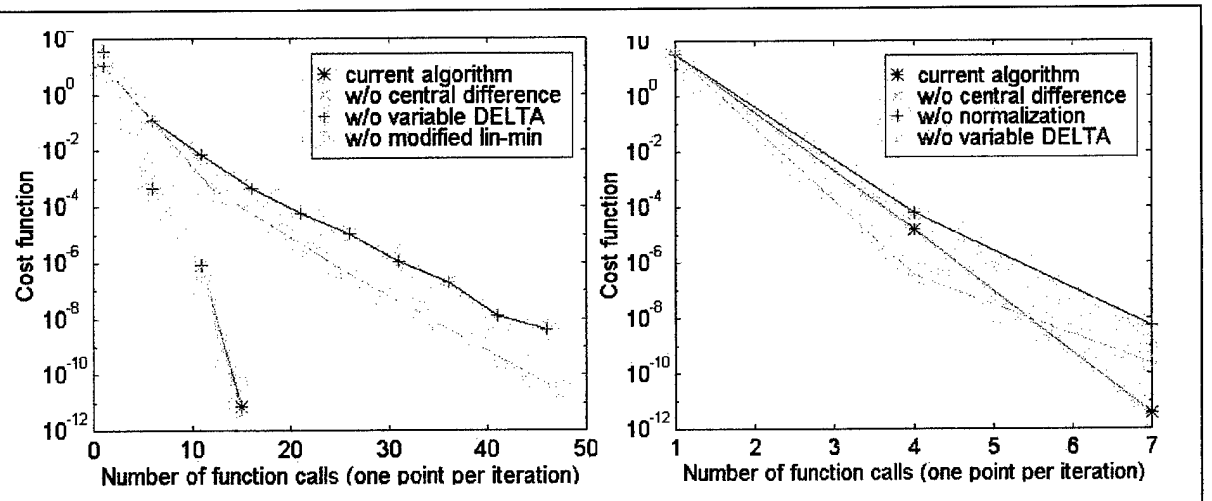

Figure 17: This shows the rate of convergence for several versions of the Conjugate Gradient (left) and the Jacobian (right) based optimization schemes.

between the various optimization schemes is the efficiency with which they "slide down the hill" to find the minimum value. This efficiency is based on the number of function calls (forward model iterations) required to produce one optimization iteration, and on the number of optimization iterations required to reach the minimum error. Figure 17 shows trials using both the Jacobian and the Conjugate Gradient methods for optimization.

Details of these techniques will be discussed in the final report and in future papers.

Concluding Remarks

This report represents the current state of this project as of September 30, 1997. Significant progress has been made between that time and the delayed filing of this report. This progress will be discussed in the final report and in future papers. Except for the delayed filing of this report, the research progress is meeting the milestone schedule and we anticipate a satisfactory conclusion of this work.

In the 4th year we anticipate the completion of ongoing work discussed above as well as an integration of the efforts in the four subsections of the project. Much of this work will be accomplished using agar phantoms and purchased ultrasound breast phantoms. As data becomes available from live patients, it will be used also. (Human patient or live animal data will not be collected as part of this research project, but we will have access to data collected as part of a separate project supervised by Dr. Roemer.) As this project concludes, a concerted effort will be made to implement the clinical system developed on the hyperthermia treatment system under development here at the University of Utah. We anticipate the publication of 4 or 5 papers resulting from this research.

References

[1] Anonymous., *JAMA*, 271:797-802, 1994.

[2] B.A. Bornstein, P.S. Zouranjian, J.L. Hansen, S.M. Fraser, L.A. Gelwan, B.A. Teicher, and G.K. Svensson, *Int. J. Radiation Oncology Biology Physics*, 25:79-85, 1993.

[3] J. Overgaard, D.G. Gonzalez, M.C.C.M. Hulshof, G. Arcangeli, O. Dahl, O. Mella, and S.M. Bentzen, *Lancet*, 345:540-543, 1995.

[4] M. Jolley, Masters Thesis, University of Utah, 1996.

[5] E.J. Halpern, Investigative Radiology, 28:598-603, 1993.

[6] G. Berger, P. Laugier, J.C. Thalabard, and J. Perrin, *Ultrasonic imaging*, 12:47-57, 1990.

[7] B.W. Dong, M. Wnag, K. Xie, and M.H. Chen, *J. Clinical Ultrasound*, 22:167-174, 1994.

[8] S.W. Flax, J.P. Norbert, G.H. Glover, F.D. Gutmann, and M. McLachlan, *Ultrasonic Imaging*, 5:95-116, 1983.

[9] B.S. Garra, M.F. Insana, T.H. Shawker, and M.A. Russell, *Radiology*, 162:61-67, 1987.

[10] M. Fink, F. Hottier, and J.F. Cardoso, *Ultrasonic Imaging*, 5:117-135, 1983.

[11] S.A. Goss, R.L. Johnson, F. Dunn, *JASA*, 64:423-457, 1978.

[12] E. Walach, A. Shmulewitz, Y. Itzchak, and Z. Heyman, *IEEE Transactions on Biomedical Engineering*, 36:211-221, 1989.

[13] E. Walach, C. N. Liu, R. C. Waag, and K. J. Parker, *IEEE Transactions on Biomedical Engineering*, BME-33:637-643, 1986.

[14] R. Kuc and M. Schwartz, *IEEE Transactions on Sonics and Ultrasonics*, SU-26:353-362, 1979.

[15] R. Kuc, *IEEE Transactions on Biomedical Engineering*, BME-27:312-319, 1980.

[16] I. Cespedes and J. Ophir, *Ultrasound in Medicine and Biology*, 16:707-717, 1990.

[17] K. J. Parker, M. S. Asztely, R. M. Lerner, E. A. Schenk, and R. C. Waag, *Ultrasound in Medicine and Biology*, 14:127-136, 1988.

[18] K. Itoh, Y. Yasuda, O. Suzuki, H. Itoh, T. Itoh, T. Jing-Wen, T. Konishi, and A. Koyano, *Journal of Clinical Ultrasound*, 16:553-562, 1988.

[19] K. Zhou, D. Zhang, C. Lin, and S. Zhu, *JASA*, 92:2532-2538, 1992.

[20] L. S. Wilson, D. E. Robinson, and B. D. Doust, *Ultrasonic Imaging*, 6:278-292, 1984.

[21] S. W. Flax, N. J. Pelc, G. H. Glover, F. D. Gutmann, and M. McLachlan, *Ultrasonic Imaging*, 5:95-116, 1983.

[22] E. J. Halpern, *Investigative Radiology*, 28:598-603, 1993.

[23] L. S. Wilson, M. L. Neale, H. E. Talhami, and M. Appleberg, *Ultrasound in Medicine and Biology*, 20:529-542, 1994.

[24] K.J. Parker, *JASA*, 74:1356-1361, 1983.

[25] M. Lyons and K.J. Parker, *IEEE Trans. Ultrasound Ferroelectrics and Freq. Control*, 35:511-521, 1988.

[26] R. Kuc, *Proc. IEEE* 73:1159-1168, 1985.